crystals

MDPI

Article

First-Principles Study on Lattice Dynamics and Thermal Conductivity of Thermoelectric Intermetallics $Fe_3Al_2Si_3$

Naoki Sato [1,*] and Yoshiki Takagiwa [2,*]

[1] International Center for Young Scientists, National Institute for Materials Science (NIMS), 1-2-1 Sengen, Tsukuba, Ibaraki 305-0047, Japan
[2] Center for Green Research on Energy and Environmental Materials, National Institute for Materials Science (NIMS), 1-2-1 Sengen, Tsukuba, Ibaraki 305-0047, Japan
* Correspondence: SATO.Naoki@nims.go.jp (N.S.); TAKAGIWA.Yoshiki@nims.go.jp (Y.T.)

Abstract: Thermoelectric materials have been expected as a critical underlying technology for developing an autonomous power generation system driven at near room temperature. For this sake, $Fe_3Al_2Si_3$ intermetallic compound is a promising candidate, though its high lattice thermal conductivity is a bottleneck toward practical applications. Herein, we have performed the first-principles calculations to clarify the microscopic mechanism of thermal transport and establish effective ways to reduce the lattice thermal conductivity of $Fe_3Al_2Si_3$. Our calculations show that the lowest-lying optical mode has a significant contribution from Al atom vibration. It should correspond to large thermal displacements Al atoms. However, these behaviors do not directly cause an increase of the 3-phonon scattering rate. The calculated lattice thermal conductivity shows a typical temperature dependence and moderate magnitude. From the calculated thermal conductivity spectrum and cumulative thermal conductivity, we can see that there is much room to reduce the lattice thermal conductivity. We can expect that heavy-element doping on Al site and controlling fine microstructure are effective strategies to decrease the lattice thermal conductivity. This work suggests useful information to manipulate the thermal transport of $Fe_3Al_2Si_3$, which will make this material closer to practical use.

Keywords: thermoelectric materials; first-principles calculations; lattice thermal conductivity

Citation: Sato, N.; Takagiwa, Y. First-Principles Study on Lattice Dynamics and Thermal Conductivity of Thermoelectric Intermetallics $Fe_3Al_2Si_3$. *Crystals* **2021**, *11*, 388. https://doi.org/10.3390/cryst11040388

Academic Editors: Mona Zebarjadi, Junxi Duan and Mousumi Mitra

Received: 12 March 2021
Accepted: 4 April 2021
Published: 7 April 2021

1. Introduction

Thermoelectric power generation (TEG) through the direct conversion of waste heat into electrical energy can contribute to a sustainable society when its efficiency dramatically improves. Recently, TEG has been attracting particular attention as one of the key technologies to establish an autonomous power supply system capable of driving internet-of-things (IoT) devices. To realize the extensive application of TEG contributing to the age of IoT called "Trillion Sensors Universe," it is desired to search for low-cost, earth-abundant, and environmentally benign thermoelectric materials which can be used as an alternative of presently commercially used Bi-Te based materials [1].

The conversion efficiency of a thermoelectric material depends on the dimensionless figure-of-merit, $ZT = S^2\sigma T/\kappa$, where S, σ, κ, and T are the Seebeck coefficient, electrical conductivity, total thermal conductivity, and absolute temperature, respectively. κ can be considered as the sum of two portions: the electronic (κ_{el}) and lattice (κ_{ph}) thermal conductivity. Recently, an Fe-Al-Si ternary intermetallic compound $Fe_3Al_2Si_3$ has been considered as a promising candidate of a novel practical thermoelectric material for low-temperature applications [2–7]. Although the ZT value of $Fe_3Al_2Si_3$ is much lower than any other practical thermoelectric materials, it has some significant advantages: (1) low-cost and non-toxic, (2) high chemical and thermal stabilities, (3) an excellent oxidation resistance, and (4) a good balance of mechanical properties [6,7]. Besides, recent efforts utilizing machine-learning to optimize power factor, $S^2\sigma$, gave a significant enhancement

of n-type value (~40%) [4]. A further improvement of power factor was recently achieved by alternating sample preparation processes [7]. A TEG module fabrication based on $Fe_3Al_2Si_3$ materials and its demonstration to drive IoT devices has already been launched in a collaborative research group between industry, government, and academia [7].

To further improve the thermoelectric performance of $Fe_3Al_2Si_3$ toward practical applications, we need to reduce the lattice thermal conductivity. The lattice thermal conductivity of undoped $Fe_3Al_2Si_3$ is 5–6 W m^{-1} K^{-1} at room temperature [2,3]. Shiota et al. reported a significant reduction to 3.5–4.5 W m^{-1} K^{-1} by Co doping on Fe site [5]. These values are relatively low compared to some other Fe-based thermoelectric materials with simple crystal structures, such as β-$FeSi_2$ (12–16 W m^{-1} K^{-1} at 300 K) [8,9], Fe_2VAl (25–28 W m^{-1} K^{-1} at 300 K) [10,11], and tetragonal $FeAl_2$ (13 W m^{-1} K^{-1} at 300 K) [12,13]. However, it is necessary to further reduce the lattice thermal conductivity of $Fe_3Al_2Si_3$-based materials considering practical use. It will be effective to establish a strategy based on a microscopic view with computational approaches. Hou et al. reported a calculation of phonon dispersion [4], but a detailed understanding of lattice dynamics and thermal transport behavior still remains unclear.

This study focuses on revealing the lattice dynamics and thermal transport mechanism of $Fe_3Al_2Si_3$ and extracting effective ways to reduce its lattice thermal conductivity based on first-principles calculations. From density functional theory (DFT)-based phonon calculations, we have identified a low-energy optical mode lying near acoustic modes which has a dominant contribution from Al atom vibration. However, it does not significantly affect the 3-phonon scattering rate though it reduces the phonon group velocity of acoustic modes near the zone boundary via an avoided-crossing effect. The calculated thermal conductivity spectrum and cumulative thermal conductivity give us a strategy that heavy-element doping on Al site and microstructure control with a length scale smaller than 500 nm effectively reduce the lattice thermal conductivity.

2. Computational Method

The $Fe_3Al_2Si_3$ phase crystallizes in a triclinic structure with space group $P\bar{1}$. The crystal structure visualized by VESTA 3 (ver. 3.5.7) [14,15] is shown in Figure S1. The crystallographic parameters of initial structure were extracted from Reference [16]. We performed first-principles calculations based on DFT. The Quantum Espresso (QE) package (ver. 6.6) [17,18] with projector-augmented wave pseudopotentials [19,20] was used as a DFT engine. The generalized gradient approximation functional with Perdew–Burke–Ernzerhof parametrization (GGA-PBE) [21] was employed for the exchange and correlation potentials. A *k*-point grid of 7 × 5 × 5 for the primitive cell and an energy cutoff of 60 Ry were used for relaxation of the crystal structure and following self-consistent field calculations.

To extract the second and third order interatomic force constants (IFC) of $Fe_3Al_2Si_3$, we used finite difference method with a 2 × 2 × 2 supercell containing 128 atoms based on the fully relaxed primitive cell to create displacement-force datasets. The magnitude of atomic displacements was set at 0.01 Å and 0.04 Å for calculating the second and third order IFCs, respectively. For the third order IFC calculation, we chose the cutoff radius as 13.8 Å for choosing triplets within which interaction is considered. A finite-temperature effect on harmonic phonon frequency [22,23] was not considered in this work because $Fe_3Al_2Si_3$ has nor phase transitions and unusually enhanced anharmonicity, as described later. The IFCs were obtained using ALAMODE (ver. 1.1.0) [24,25] code, which is a package designed for analyzing lattice anharmonicity and lattice thermal conductivity of solids. The phonon dispersion relation and density of states (DOS) were calculated from the second order IFC. The sampling grid used for summation was 15 × 10 × 9. Dielectric constant and Born effective charge were calculated in the perturbation framework implemented in QE package. The anharmonic phonon linewidth and scattering rate are computed from the third order IFC by ALAMODE and then used to calculate the lattice thermal conductivity by solving phonon Boltzmann transport equation within the single mode relaxation time

approximation. The sampling grid 15 × 10 × 9 was applied after confirming convergence of the calculated lattice thermal conductivity with respect to the grid density.

3. Results and Discussion

Hou et al. recently reported that GGA-PBE functional reproduces the experimental lattice parameters of $Fe_3Al_2Si_3$ better than PBEsol and SCAN functionals [26]. Moreover, the calculated bulk modulus, Young's modulus, shear modulus, and Poisson's ratio were in good agreement with the experimental ones with GGA-PBE functional [26]. Thus, we applied GGA-PBE functional for an evaluation of lattice dynamics of $Fe_3Al_2Si_3$ in this study. The optimized lattice parameters of $Fe_3Al_2Si_3$ together with some previous calculated and experimental reports are listed in Table 1. Our calculation using QE package reproduces Reference [26] within 1% and is in good agreement with the experimental data.

Table 1. Calculated lattice parameters (a, b, and c in Å, and α, β, and γ in degree) of optimized structure of $Fe_3Al_2Si_3$ [26]. Experimental ones [4,16,27] are also listed for comparison.

Parameter	Calculated		Experimental		
	This Study (QE, PBE)	Reference [26] (VASP, PBE)	Reference [4]	Reference [16]	Reference [27]
a	4.6011	4.6032	4.5995	4.684	4.6512
b	6.3244	6.3256	6.3352	6.325	6.3261
c	7.4578	7.4594	7.521	7.498	7.499
α	101.91	101.90	101.827	100.99	101.375
β	106.78	106.79	106.427	105.6	105.923
γ	100.59	100.59	100.729	101.62	101.237

Figure 1 shows the calculated phonon dispersion curve together with the phonon DOS of $Fe_3Al_2Si_3$. The curve consists of three acoustic and 45 optical branches. We included the non-analytical term correction to dynamical matrix by calculating dielectric constant and BEC. As a result, we observed longitudinal optical-transverse optical (LO-TO) splitting near the zone center induced by long-range Coulomb interaction. The atomic decomposed partial DOS has many peaks in wide frequency range due to the wide variety of bond length and corresponding second order IFC. Figure 2 shows the total and site-decomposed phonon DOS of $Fe_3Al_2Si_3$. The label of each crystallographic sites corresponds to the visualization of crystal structure shown in Figure S1. It is remarkable that the lowest-lying optical (LLO) mode, which is observed at about 3.8 THz at the zone center, has large contribution from the lightest Al-atom vibration. As shown in Figure 2b, both of Al1 and Al2 site have significant contribution to the LLO mode though Al2 site exhibits twice higher peak. In the mid- and high-frequency region, Al1 and Al2 sites have separate peaks. As compared to Al-sites, three Fe-sites have peaks at similar frequency region, as shown in Figure 2c. The highest dispersive optical mode has a large contribution from Si1 site, as shown in Figure 2d. These behaviors were also reported by Hou et al. [4] The LLO and acoustic modes show avoided-crossing behavior in some directions, such as Γ–Y, Γ–Z, Γ–U. This kind of avoided-crossing has been observed in some cage-like materials, such as filled Skutterudites [28,29] and clathrates [30–32], with strongly anharmonic lattice vibration, so-called rattling. The avoided-crossing typically causes a significant softening of acoustic modes and results in a reduced phonon group velocity near the zone boundary. Besides, coexistence of the LLO and acoustic modes in similar energy region enhances interaction between acoustic and optical modes and increases 3-phonon scattering rates. Thus, these features observed in $Fe_3Al_2Si_3$ could play a significant role in thermal transport behavior.

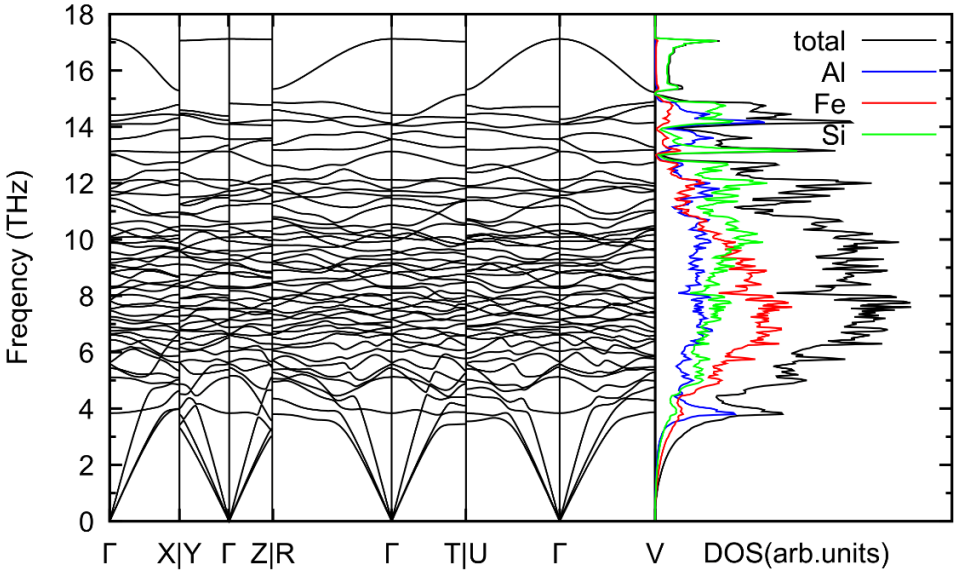

Figure 1. Phonon dispersion curve and phonon density of states (DOS) of $Fe_3Al_2Si_3$.

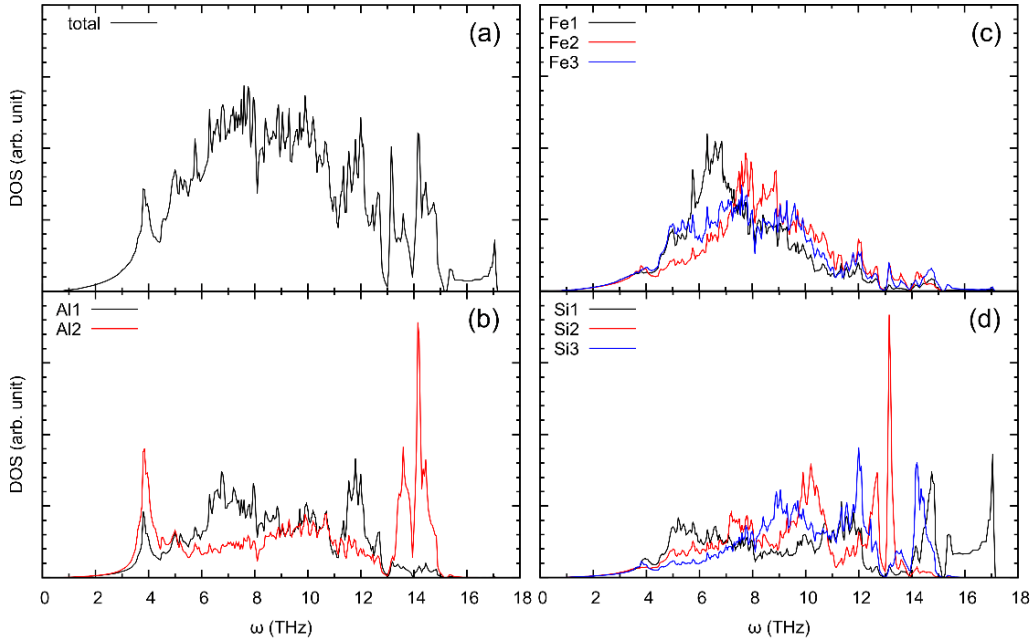

Figure 2. (**a**) Total phonon DOS and site-decomposed partial phonon DOS for (**b**) Al-, (**c**) Fe-, and (**d**) Si-sites, respectively.

Figure 3 shows the temperature dependence of calculated mean square displacement (MSD) of each crystallographic site. We can clearly observe that the magnitude of Al2 site in the *z*-direction is much larger than the other sites and directions. This corresponds to that the flat LLO mode has largest contribution from Al2 site. Besides, the magnitude of displacement eigenvector of the LLO mode is the largest for Al2 site in the *z*-direction. A low potential barrier surrounding Al2 atom, which can be derived from soft bonding environment, should cause these features. There are some previous reports on large MSD of guest atom in the cage-like materials which exhibit large anharmonicity and low lattice thermal conductivity. We should note that the large displacement itself does not necessarily correspond to large phonon anharmonicity.

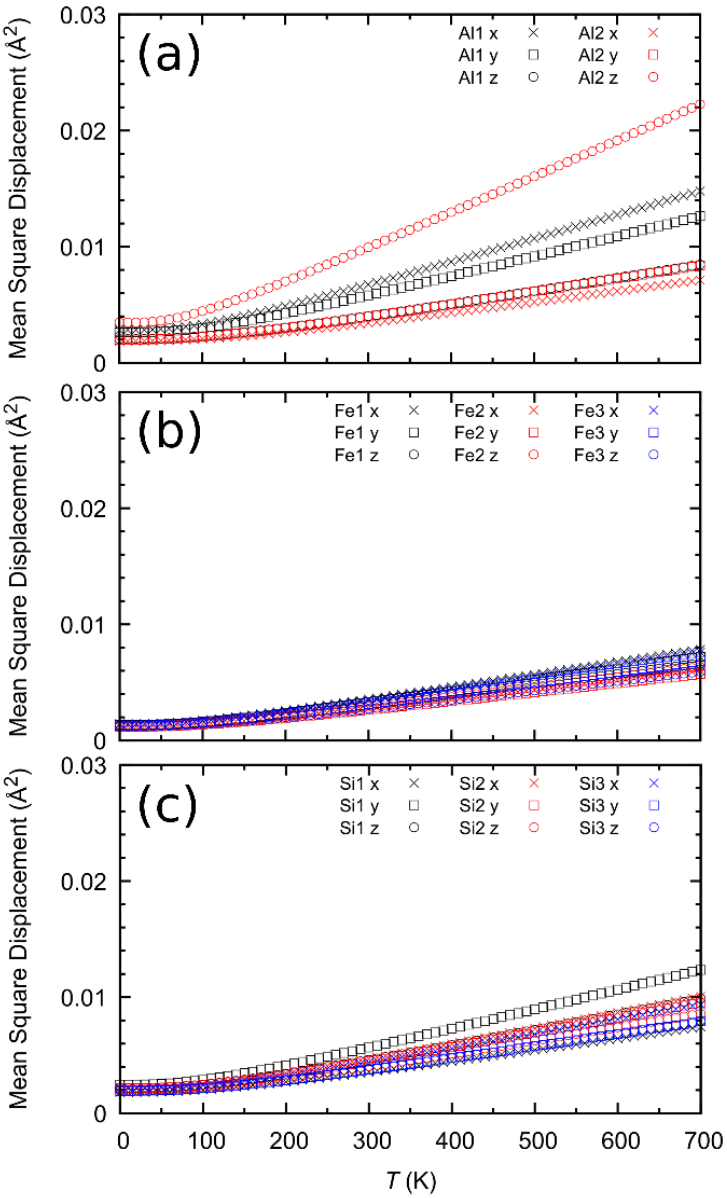

Figure 3. Temperature dependence of atomic mean square displacement for (**a**) Al-, (**b**) Fe-, and (**c**) Si-sites, respectively.

Figure 4a shows the phonon group velocity of all branches. The magnitude of group velocity rapidly drops at around 4 THz, which can be attributed to the softening of acoustic mode coming from avoided-crossing. However, higher group velocity of optical modes than acoustic modes are also observed at around 4 THz, which comes from some dispersive branches such as Γ–Y region. Thus, the optical modes should have non-negligible effect on thermal transport in $Fe_3Al_2Si_3$.

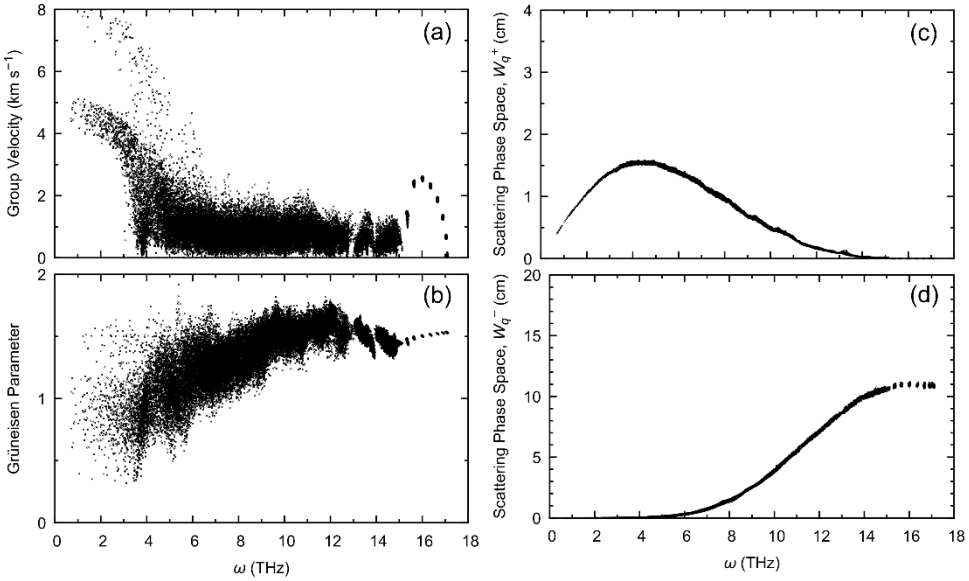

Figure 4. (**a**) Phonon group velocity, (**b**) mode Grüneisen parameter, and 3-phonon scattering phase space at 300 K for (**c**) absorption and (**d**) emission processes, respectively.

Figure 4b shows the mode Grüneisen parameter, which estimates lattice anharmonicity. Some low thermal conductivity materials with large anharmonicity, such as PbTe, exhibit large (>10) mode Grüneisen parameter at around zone-center [33,34]. On the other hand, $Fe_3Al_2Si_3$ exhibits relatively small mode Grüneisen parameter at overall frequency region. Thus, the flat LLO mode mentioned above does not have a distinctive anharmonic feature unlike resonant mode observed with rattling. Figure 4c,d shows the 3-phonon scattering phase space (SPS) at 300 K for absorption and emission processes, respectively. The SPS is given as

$$W_q^{\pm} = \frac{1}{N}\sum_{q',q''}\left\{\begin{array}{c} n_{q''} - n_{q'} \\ n_{q'} + n_{q''} + 1 \end{array}\right\}\delta\left(\omega_q - \omega_{q'} \pm \omega_{q''}\right) \quad (1)$$

where W_q^+ and W_q^- are the SPS corresponding to absorption and emission processes of phonon mode q, respectively. Here, the variable q is defined by $q = (\boldsymbol{q}, j)$ and $-q = (-\boldsymbol{q}, j)$ where $\boldsymbol{q}$ and j are the wave vector and the branch index of phonon modes. n_q is the Bose–Einstein distribution function. The SPS estimates the amount of 3-phonon scattering channel satisfying energy and momentum conservation and is roughly proportional to the scattering rate. The SPS for absorption process has a broad peak at around 4 THz, which can be considered as an increase of interaction between acoustic and optical modes. On the other hand, we can observe no characteristic feature in the low-frequency range for emission process. Overall, $Fe_3Al_2Si_3$ is not a highly anharmonic crystal which shows high phonon scattering rate despite its soft bonding environment of Al atom.

Figure 5 shows the calculated lattice thermal conductivity considering only 3-phonon scattering processes in each crystallographic direction (xx, yy, and zz). The values of 10 W m^{-1} K^{-1} in yy and zz directions and 9 W m^{-1} K^{-1} in xx direction at 300 K are relatively high compared to practical thermoelectric materials [35]. The temperature dependence shows a typical decay behavior, $\kappa_{ph} \propto T^{-1}$. Three experimental values of stoichiometric and non-stoichiometric polycrystalline samples from References [2,3] are also shown in Figure 5. All the experimental values significantly deviate from the calculated results. Because the experimental values are extracted from the polycrystalline samples, grain boundary should have significant effect on the lattice thermal conductivity mainly at low temperature region. Besides, point defect scattering also should reduce the lattice thermal conductivity. As shown in Figure S2, the defect formation energies of Al-on-Si and Si-on-Al antisite defects are so low that the defects can be easily formed. Actually,

it is experimentally confirmed that the $Fe_3Al_2Si_3$ phase crystallizes in wide composition range [4,16]. Thus, the synthesized polycrystalline samples of $Fe_3Al_2Si_3$ should contain large amount of antisite defects, which results in a significant reduction of the lattice thermal conductivity. At high temperature range, the experimental value increases with increasing temperature. This should be derived from an excitation of minority carrier since $Fe_3Al_2Si_3$ is a narrow-gap semiconductor with the band gap of about 0.2 eV [2,3,26].

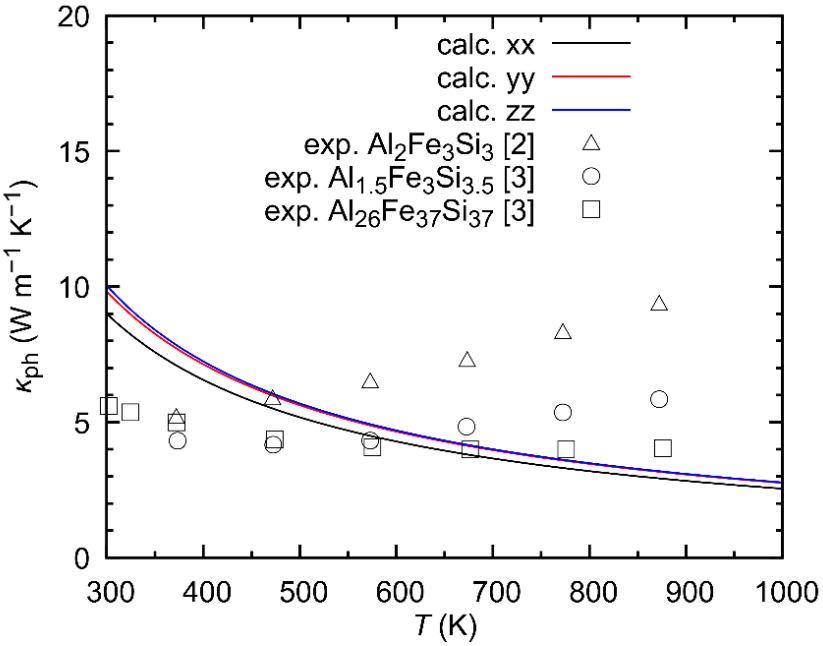

Figure 5. Temperature dependence of calculated lattice thermal conductivity together with experimental value of stoichiometric and non-stoichiometric polycrystalline samples from References [2,3].

To gain further insight into a reduction of the lattice thermal conductivity of $Fe_3Al_2Si_3$, we calculated the thermal conductivity spectrum in phonon frequency space, as shown in Figure 6a. The spectrum has a highest peak at acoustic mode region, which is a typical behavior. Moreover, we can see that optical modes from 4 THz to 8 THz have significant contribution to the lattice thermal conductivity. This corresponds to that the optical modes have high group velocity as well as the acoustic modes. From the discussion above, we can suggest that a heavy-element doping/alloying on Al sites is especially effective to further lower the energy of LLO mode, which in turn enhances the effect of avoided-crossing and reduces the group velocity near the zone-boundary. It should also introduce the point defect scattering. A screening of effective dopants and quantitative estimation of the doping effects are possible future work.

Figure 6b shows the cumulative thermal conductivity normalized by the calculated bulk value at 300 K. From the cumulative thermal conductivity, we can gain information on the length scale of phonons which are dominant for the thermal transport. The calculated results show that phonons with the mean free path $l < 500$ nm make a significant contribution to the thermal transport. For example, phonons with $l > 33$ nm, 39 nm, and 50 nm carry 50% of the heat in a bulk material in *xx*, *yy*, and *zz* directions, respectively. In other words, controlling the microstructure size with these length scales would have potential to reduce the lattice thermal conductivity in half. This information, together with the doping strategy mentioned above, gives indication that there is room to reduce the lattice thermal conductivity and improve thermoelectric efficiency of $Fe_3Al_2Si_3$.

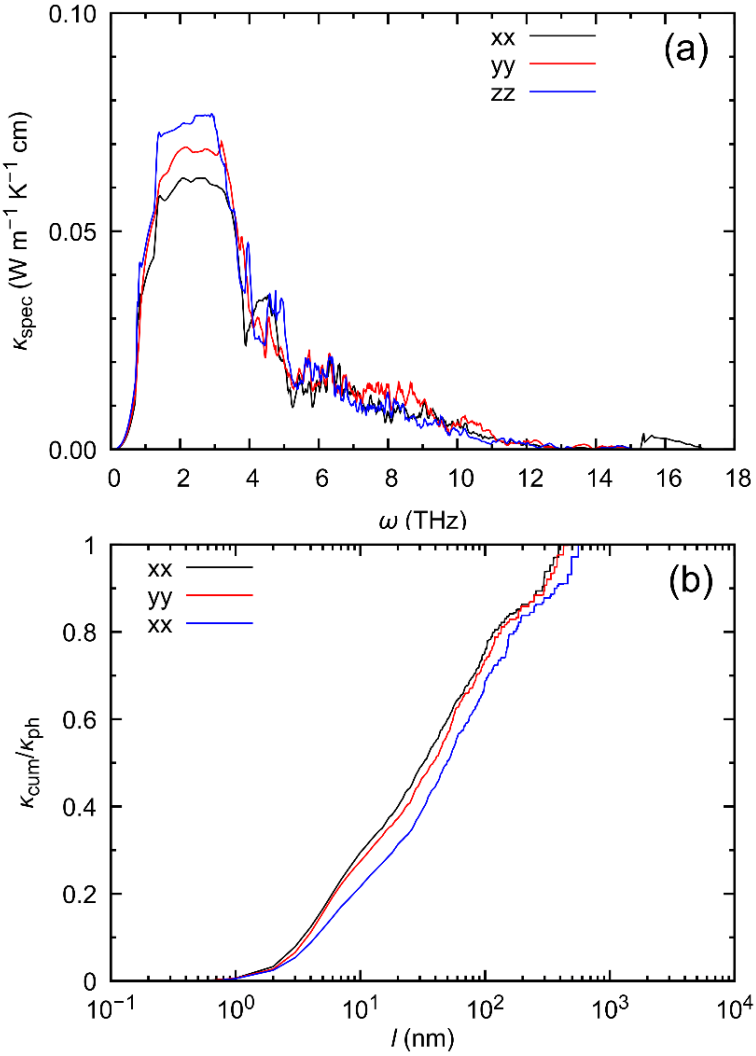

Figure 6. (**a**) Thermal conductivity spectrum in phonon frequency space and (**b**) cumulative thermal conductivity normalized by calculated bulk lattice thermal conductivity with respect to phonon mean free path at 300 K.

4. Conclusions

By using DFT-based calculations, we have investigated the lattice dynamics and thermal conductivity of $Fe_3Al_2Si_3$, which has been expected as a novel low-cost and non-toxic thermoelectric material. The lowest-lying optical mode, which was observed near the acoustic modes, has large contribution from Al2 site. Besides, Al2 site shows large thermal displacement compared to the other atomic sites. However, these features are found not to have significantly favorable effects on the phonon anharmonicity and scattering rate. As a result, $Fe_3Al_2Si_3$ has an intrinsically high lattice thermal conductivity. From the calculated thermal conductivity spectrum, we obtained a strategy that heavy-element doping on Al site can alter the phonon dispersion in low-frequency range and reduce phonon group velocity. Further, an effective length scale of microstructure was clarified from the cumulative thermal conductivity. This study gives basic information on the phonons, and the strategies obtained here should awaken further experimental efforts to improve the thermoelectric performance of $Fe_3Al_2Si_3$ towards realizing practical IoT devices.

Supplementary Materials: The following are available online at https://www.mdpi.com/article/10.3390/cryst11040388/s1. Description of the calculation of defect formation energy; Figure S1:

Visualized crystal structure of $Fe_3Al_2Si_3$; Figure S2: Calculated defect formation energies of antisite defects (Al_{Si1}, Al_{Si2}, Al_{Si3}, Si_{Al1}, and Si_{Al2}) as a function of Fermi energy for the boundary condition of (a) $Fe_3Al_2Si_3$-Al_3Fe_2Si-$Al_{79}(Fe_{13}Si_9)_2$, (b) $Fe_3Al_2Si_3$-Al_3Fe_2Si-$AlFe_2Si$, (c) $Fe_3Al_2Si_3$-$Al_{53}Fe_{17}Si_{12}$-$Al_{79}(Fe_{13}Si_9)_2$, (d) $Fe_3Al_2Si_3$-$Al_{53}Fe_{17}Si_{12}$-$FeSi_2$, (e) $Fe_3Al_2Si_3$-$AlFe_2Si$-$FeSi$, and (f) $Fe_3Al_2Si_3$-$FeSi$-$FeSi_2$ regions. The Fermi energy is referenced to the valence band maximum, and the vertical dashed black line indicates the band gap region within the GGA-PBE level.

Author Contributions: N.S. and Y.T. conceived the study. N.S. performed the calculations and analyzed the data. N.S. and Y.T. wrote, reviewed, and edited the manuscript. All authors have read and agreed to the published version of the manuscript.

Funding: This work was supported by the Japan Society for the Promotion of Science (JSPS KAKENHI grant nos. 19H05821 and 20H02469).

Acknowledgments: N.S. would like to acknowledge the ICYS fellowship in NIMS, Japan. The computation in this work has been performed using Numerical Materials Simulator at NIMS.

Conflicts of Interest: The authors declare no conflict of interest.

References

1. Goldsmid, H. Bismuth Telluride and Its Alloys as Materials for Thermoelectric Generation. *Materials* **2014**, *7*, 2577–2592. [CrossRef]
2. Shiota, Y.; Muta, H.; Yamamoto, K.; Ohishi, Y.; Kurosaki, K.; Yamanaka, S. A new semiconductor $Al_2Fe_3Si_3$ with complex crystal structure. *Intermetallics* **2017**, *89*, 51–56. [CrossRef]
3. Takagiwa, Y.; Isoda, Y.; Goto, M.; Shinohara, Y. Electronic structure and thermoelectric properties of narrow-band-gap intermetallic compound $Al_2Fe_3Si_3$. *J. Therm. Anal. Calorim.* **2018**, *131*, 281–287. [CrossRef]
4. Hou, Z.; Takagiwa, Y.; Shinohara, Y.; Xu, Y.; Tsuda, K. Machine-Learning-Assisted Development and Theoretical Consideration for the $Al_2Fe_3Si_3$ Thermoelectric Material. *ACS Appl. Mater. Interfaces* **2019**, *11*, 11545–11554. [CrossRef] [PubMed]
5. Shiota, Y.; Yamamoto, K.; Ohishi, Y.; Kurosaki, K.; Muta, H. Thermoelectric Properties of Co- and Mn-Doped $Al_2Fe_3Si_3$. *J. Electron. Mater.* **2019**, *48*, 475–482. [CrossRef]
6. Takagiwa, Y.; Shinohara, Y. A practical appraisal of thermoelectric materials for use in an autonomous power supply. *Scr. Mater.* **2019**, *172*, 98–104. [CrossRef]
7. Takagiwa, Y.; Ikeda, T.; Kojima, H. Earth-Abundant Fe–Al–Si Thermoelectric (FAST) Materials: From Fundamental Materials Research to Module Development. *ACS Appl. Mater. Interfaces* **2020**, *12*, 48804–48810. [CrossRef]
8. Waldecker, G.; Meinhold, H.; Birkholz, U. Thermal conductivity of semiconducting and metallic $FeSi_2$. *Phys. Status Solidi* **1973**, *15*, 143–149. [CrossRef]
9. Kim, S.W.; Cho, M.K.; Mishima, Y.; Choi, D.C. High temperature thermoelectric properties of p- and n-type β-$FeSi_2$ with some dopants. *Intermetallics* **2003**, *11*, 399–405. [CrossRef]
10. Lue, C.S.; Kuo, Y.K. Thermoelectric properties of the semimetallic Heusler compounds $Fe_{2-x}V_{1+x}M$ (M = Al, Ga). *Phys. Rev. B* **2002**, *66*, 085121. [CrossRef]
11. Nishino, Y.; Deguchi, S.; Mizutani, U. Thermal and transport properties of the Heusler-type $Fe_2VAl_{1-x}Ge_x$ ($0 \leq x \leq 0.20$) alloys: Effect of doping on lattice thermal conductivity, electrical resistivity, and Seebeck coefficient. *Phys. Rev. B* **2006**, *74*, 115115. [CrossRef]
12. Tobita, K.; Sato, N.; Katsura, Y.; Kitahara, K.; Nishio-Hamane, D.; Gotou, H.; Kimura, K. High-pressure synthesis of tetragonal iron aluminide $FeAl_2$. *Scr. Mater.* **2017**, *141*, 107–110. [CrossRef]
13. Tobita, K.; Kitahara, K.; Katsura, Y.; Sato, N.; Nishio-Hamane, D.; Gotou, H.; Kimura, K. Phase stability and thermoelectric properties of semiconductor-like tetragonal $FeAl_2$. *Sci. Technol. Adv. Mater.* **2019**, *20*, 937–948. [CrossRef]
14. Momma, K.; Izumi, F. VESTA 3 for three-dimensional visualization of crystal, volumetric and morphology data. *J. Appl. Crystallogr.* **2011**, *44*, 1272–1276. [CrossRef]
15. VESTA. Available online: https://jp-minerals.org/vesta/en/ (accessed on 4 April 2021).
16. Marker, M.C.J.; Skolyszewska-Kühberger, B.; Effenberger, H.S.; Schmetterer, C.; Richter, K.W. Phase equilibria and structural investigations in the system Al–Fe–Si. *Intermetallics* **2011**, *19*, 1919–1929. [CrossRef]
17. Giannozzi, P.; Baroni, S.; Bonini, N.; Calandra, M.; Car, R.; Cavazzoni, C.; Ceresoli, D.; Chiarotti, G.L.; Cococcioni, M.; Dabo, I.; et al. QUANTUM ESPRESSO: A modular and open-source software project for quantum simulations of materials. *J. Phys. Condens. Matter* **2009**, *21*, 395502. [CrossRef] [PubMed]
18. QUANTUM ESPRESSO. Available online: https://www.quantum-espresso.org/ (accessed on 4 April 2021).
19. Blöchl, P.E. Projector augmented-wave method. *Phys. Rev. B* **1994**, *50*, 17953–17979. [CrossRef]
20. Kresse, G.; Joubert, D. From ultrasoft pseudopotentials to the projector augmented-wave method. *Phys. Rev. B* **1999**, *59*, 1758–1775. [CrossRef]
21. Perdew, J.P.; Burke, K.; Ernzerhof, M. Generalized Gradient Approximation Made Simple. *Phys. Rev. Lett.* **1996**, *77*, 3865–3868. [CrossRef] [PubMed]

22. Szymanski, N.J.; Walters, L.N.; Hellman, O.; Gall, D.; Khare, S.V. Dynamical stabilization in delafossite nitrides for solar energy conversion. *J. Mater. Chem. A* **2018**, *6*, 20852–20860. [CrossRef]
23. Tadano, T.; Tsuneyuki, S. Self-consistent phonon calculations of lattice dynamical properties in cubic $SrTiO_3$ with first-principles anharmonic force constants. *Phys. Rev. B* **2015**, *92*, 054301. [CrossRef]
24. Tadano, T.; Gohda, Y.; Tsuneyuki, S. Anharmonic force constants extracted from first-principles molecular dynamics: Applications to heat transfer simulations. *J. Phys. Condens. Matter* **2014**, *26*, 225402. [CrossRef]
25. ALAMODE. Available online: https://alamode.readthedocs.io/en/latest/index.html (accessed on 4 April 2021).
26. Hou, Z.; Takagiwa, Y.; Shinohara, Y.; Xu, Y.; Tsuda, K. First-principles study of electronic structures and elasticity of $Al_2Fe_3Si_3$. *J. Phys. Condens. Matter* **2021**. accepted manuscript. [CrossRef] [PubMed]
27. Yanson, T.I.; Manyako, M.B.; Bodak, O.I.; German, N.V.; Zarechnyuk, O.S.; Cerný, R.; Pacheco, J.V.; Yvon, K. Triclinic $Fe_3Al_2Si_3$ and Orthorhombic $Fe_3Al_2Si_4$ with New Structure Types. *Acta Crystallogr. Sect. C Cryst. Struct. Commun.* **1996**, *52*, 2964–2967. [CrossRef]
28. Li, W.; Mingo, N. Ultralow lattice thermal conductivity of the fully filled skutterudite $YbFe_4Sb_{12}$ due to the flat avoided-crossing filler modes. *Phys. Rev. B-Condens. Matter Mater. Phys.* **2015**, *91*, 144304. [CrossRef]
29. Lee, C.H.; Hase, I.; Sugawara, H.; Yoshizawa, H.; Sato, H. Low-Lying Optical Phonon Modes in the Filled Skutterudite $CeRu_4Sb_{12}$. *J. Phys. Soc. Jpn.* **2006**, *75*, 123602. [CrossRef]
30. Tse, J.S.; Shpakov, V.P.; Murashov, V.V.; Belosludov, V.R. The low frequency vibrations in clathrate hydrates. *J. Chem. Phys.* **1997**, *107*, 9271–9274. [CrossRef]
31. Christensen, M.; Abrahamsen, A.B.; Christensen, N.B.; Juranyi, F.; Andersen, N.H.; Lefmann, K.; Andreasson, J.; Bahl, C.R.H.; Iversen, B.B. Avoided crossing of rattler modes in thermoelectric materials. *Nat. Mater.* **2008**, *7*, 811–815. [CrossRef] [PubMed]
32. Tadano, T.; Tsuneyuki, S. Quartic Anharmonicity of Rattlers and Its Effect on Lattice Thermal Conductivity of Clathrates from First Principles. *Phys. Rev. Lett.* **2018**, *120*, 105901. [CrossRef] [PubMed]
33. Esfarjani, K.; Chen, G.; Stokes, H.T. Heat transport in silicon from first-principles calculations. *Phys. Rev. B* **2011**, *84*, 085204. [CrossRef]
34. Shiomi, J.; Esfarjani, K.; Chen, G. Thermal conductivity of half-Heusler compounds from first-principles calculations. *Phys. Rev. B* **2011**, *84*, 104302. [CrossRef]
35. Snyder, G.J.; Toberer, E.S. Complex thermoelectric materials. *Nat. Mater.* **2008**, *7*, 105–114. [CrossRef] [PubMed]